동적 고성능과 최대 전력 효율을 위한 유도 전동기 회전자 속도와 회전자 자속의 선형 비간섭 제어

김 동 일*, 하 인 중, 고 명 삼, 박 재 화

서울대학교 제어계측공학과
로보틱스 지능시스템 실험실

LINEAR DECOUPLING CONTROL OF ROTOR SPEED AND ROTOR FLUX IN INDUCTION MOTOR FOR HIGH DYNAMIC PERFORMANCE AND MAXIMAL POWER EFFICIENCY

Dong-Il Kim, In-Joong Ha, Myoung-Sam Ko, and Jae-Wha Park

Robotics and Intelligent Systems Laboratory
Depart. of Control and Instrumentation Engr.
Seoul National University

Abstract : We attempt to achieve both high dynamic performance and maximal power efficiency by means of linear decoupling of rotor speed (or motor torque) and rotor flux. The induction motor with our controller possesses the input-output dynamic characteristics of a linear system such that the rotor speed (or motor torque) and the rotor flux are decoupled. The rotor speed (or motor torque) responses are not affected by abrupt changes in the rotor flux and vice versa. The rotor flux need not be measured but is estimated by the well-known flux simulator. The effect of large variation in the rotor resistance on the control performances is minimized by employing a parameter adaptation method. To illuminate the significance of our work, we present simulation and experimental results as well as mathematical performance analyses.

1. Introduction

Recently, many researchers have tried to improve further the so called vector control (or field oriented control) method pioneered by Blaschke [1]. In particular, the controllers proposed by Kuroe and Haneda [2], Koyama et al. [3], Ohnishi et al. [4], Lorenz and Lawson [5], and Ho and Sen [6] force induction motors to behave like DC motors by controlling rotor fluxes constant. On the other hand, Luca and Ulivi [7], Krzeminski [8], and Kim et al. [9] have shown that the dynamic equations of induction motors can be fully linearized by utilizing the recently developed nonlinear feedback control theories [10]-[14]. In their control methods, the rotor flux need not be kept constant. However, for exact linearization by nonlinear feedback control, the parameters of the induction motor must be precisely known and the accurate information of the motor flux is required.

In practice, rotor fluxes can be measured through direct sensing of air gap fluxes with flux-sensing coils or Hall-probes [1,15]. However, it is more cost-effective to estimate rotor fluxes based on the rotor circuit equations [3,9,16,17]. On the other hand, the parameters of the induction motor (in particular, rotor resistance) change widely with temperature and/or magnetic saturation. Variations in parameters cause deterioration of both dynamic and steady-state performance of induction motor control systems [18]. Efficient identification algorithms for the rotor resistance can be found in recent researches [3,19].

Beside dynamic performance, there are other important factors to be taken into account in the controller design of induction motors. Among them is power efficiency. Induction motors in particular consume a large fraction of all electric power in industrial fields, so control for high power efficiency is required to reduce energy losses. Various control methods for high power efficiency have been proposed by Kusko and Galler [20], Park and Sul [21], and Murata et al. [22]. However, these control methods for high power efficiency can not control the induction motor to behave like a linear system or may sacrifice the dynamic performance of rotor speed.

In this paper, we attempt to control the induction motor with high dynamic performance and maximal power efficiency by means of linear decoupling of rotor speed and rotor flux. For maximal power efficiency, the rotor flux need be adjusted continuously depending on rotor speed commands. Due to linear decoupling of rotor speed and rotor flux, this can be successfully done without affecting rotor speed responses. The rotor speed responses to input commands follow the input-output dynamic characteristics of a linear system. Direct measurement of the rotor flux is not required to achieve linear decoupling of rotor speed and rotor flux. Performances of our control scheme are robust with respect to variations of induction motor parameters since an identification algorithm for the rotor resistance is used. The prior results do not necessarily possess all these features. We present the mathematical performance analysis of our control scheme in the presence of uncertainty in the rotor resistance. The prior results closely related to ours are discussed at length. Both simulation and experimental results were carried out to demonstrate the practical significance of our results. In particular, our experimental results show that recently developed nonlinear feedback control techniques are of practical use.

2. Controller design

In the d-q coordinate frame rotating synchronously with an angular speed ω_s, the dynamic equations of a p-pole pair induction motor are described by:

$$\begin{aligned}
\dot{i}_{ds} &= -a_1 i_{ds} + \omega_s i_{qs} + a_2 \phi_{dr} + p a_3 \omega_r \phi_{qr} + cV_{ds}, \\
\dot{i}_{qs} &= -\omega_s i_{ds} - a_1 i_{qs} - p a_3 \omega_r \phi_{dr} + a_2 \phi_{qr} + cV_{qs}, \\
\dot{\phi}_{dr} &= -a_4 \phi_{dr} + a_5 i_{ds} + (\omega_s - p\omega_r)\phi_{qr}, \\
\dot{\phi}_{qr} &= -a_4 \phi_{qr} + a_5 i_{qs} - (\omega_s - p\omega_r)\phi_{dr}, \\
\dot{\omega}_r &= (-D\omega_r + T_e - T_L)/J,
\end{aligned} \tag{2.1}$$

where T_e is the generated torque given by

$$T_e = K_T(\phi_{dr} i_{qs} - \phi_{qr} i_{ds}). \tag{2.2}$$

Here, V_{ds}, V_{qs}, and ω_s are the control inputs. The constants c, D, J, K_T, and a_i, $i = 1, \cdots, 5$ are the parameters of the induction motor. Definitions of the symbols and notations used frequently in our developments are given in Nomenclature.

It is well-known that, if ω_s is chosen as

$$\omega_s = p\omega_r + a_5 i_{qs}/\phi_{dr} \tag{2.3}$$

the dynamic behavior of the induction motor after sufficient time is governed by

$$\begin{aligned}
\dot{i}_{ds} &= -a_1 i_{ds} + \omega_s i_{qs} + a_2 \phi_{dr} + cV_{ds}, \\
\dot{i}_{qs} &= -\omega_s i_{ds} - a_1 i_{qs} - p a_3 \omega_r \phi_{dr} + cV_{qs}, \\
\dot{\phi}_{dr} &= -a_4 \phi_{dr} + a_5 i_{ds}, \\
\dot{\omega}_r &= (-D\omega_r + K_T \phi_{dr} i_{qs} - T_L)/J
\end{aligned} \tag{2.4}$$

and the d-q coordinate frame coincides with the coordinate frame rotating synchronously with the rotor flux vector. Take the input u and the output $\vec{y}$ by

$$u=\begin{bmatrix}V_{ds}\\ V_{qs}\end{bmatrix}=\begin{bmatrix}-\omega_s i_{qs}/c\\ p\omega_r(i_{ds}+a_3\phi_{dr})/c\end{bmatrix}+\begin{bmatrix}1 & 0\\ 0 & 1/\phi_{dr}\end{bmatrix}\vec{u}, \tag{2.5}$$

$$\vec{y}=[\phi_{dr}\quad \omega_r]^T$$

Then, the input-output dynamic behavior of the system (2.4) with (2.5) is the same as that of the following decoupled linear system:

$$\begin{aligned}\dot{\bar{z}}_1&=\bar{A}_1\bar{z}_1+\bar{b}_1\bar{u}_1, & \bar{y}_1&=\bar{c}_1\bar{z}_1,\\ \dot{\bar{z}}_2&=\bar{A}_2\bar{z}_2+\bar{b}_2\bar{u}_2+\bar{E}T_L, & \bar{y}_2&=\bar{c}_2\bar{z}_2,\end{aligned} \tag{2.6}$$

where the detailed structures of $\bar{A}_i$, $\bar{b}_i$, $\bar{c}_i$, $i=1, 2$, and $\bar{E}$ are given in Appendix A. This can be easily seen by noting that the state-space coordinate change:

$$\begin{aligned}\bar{z}=[\bar{z}_1^T\quad \bar{z}_2^T]^T&=[\bar{z}_{11}\quad \bar{z}_{12}\quad \bar{z}_{21}\quad \bar{z}_{22}]^T\\ &=[i_{ds}\quad \phi_{dr}\quad \phi_{dr}i_{qs}\quad \omega_r]^T\end{aligned} \tag{2.7}$$

takes the nonlinear system consisting of (2.4) and (2.5) to the decoupled linear system (2.6) and by recalling that the input-output dynamic characteristics are invariant with respect to the state transformation.

The block diagram representation of the system (2.6) is shown in the dashed block of Fig.2.1. Since the system (2.6) is linear and decoupled, the rotor speed (or the generated torque) and the rotor flux can be independently controlled. Furthermore, well-developed linear control theories can be directly applied to achieve high dynamic performance. Thus, this approach (which is well-known as feedback linearization with input-output decoupling [14,23] facilitates the controller design of induction motors which have highly nonlinear dynamics. In fact, it can be shown that the system (2.4) satisfies the conditions for feedback linearization with input-output decoupling in the paper by Tarn et al. [23]. Therefore, the feedback control law (2.5) and the state transformation (2.7) for feedback linearization with input-output decoupling could be obtained by solving the set of partial differential equations given in the above literature. However, (2.5) and (2.7) can be much more easily found by physical insight.

Unfortunately, this approach faces some difficulties in its practical implementation. First, the controller consisting of (2.3) and (2.5) needs flux sensors. However, it is impractical because there exists reluctance to install flux-sensing coils or Hall effect transducers in the stator of the induction motor. Second, the rotor resistance R_r varies largely with the machine temperature. Since the a_i are linear functions of R_r, values of those parameters deviate largely from their nominal values as the machine temperature rises.

To overcome these difficulties, we modify the controller in (2.3), (2.5) as follows:

$$u=\begin{bmatrix}V_{ds}\\ V_{qs}\end{bmatrix}=\begin{bmatrix}-\omega_s i_{qs}/c+\bar{u}_1\\ p\omega_r(i_{ds}+a_3\hat{\phi}_{dr})/c+\bar{u}_2/\hat{\phi}_{dr}\end{bmatrix}, \tag{2.8}$$

$$\omega_s=p\omega_r+\hat{a}_5 i_{qs}/\hat{\phi}_{dr}$$

where $\hat{\phi}_{dr}$ is the estimated value of ϕ_{dr} obtained from the well-known simulator for ϕ_{dr} [3,9]:

$$\dot{\hat{\phi}}_{dr}=-\hat{a}_4\hat{\phi}_{dr}+\hat{a}_5 i_{ds}. \tag{2.9}$$

The parameters $\hat{a}_4$, $\hat{a}_5$ which appear in (2.8), (2.9) represent the estimated values of a_4, a_5, respectively. These parameters are successively updated by the identification algorithm for the rotor resistance, which will be presented in Section 3. Finally, the new inputs $\bar{u}_1$, $\bar{u}_2$ in (2.8) are chosen as

$$\begin{aligned}\bar{u}_1&=K_{pd}(\tilde{u}_1-i_{ds})+K_{id}\int_0^t(\tilde{u}_1-i_{ds})dt,\\ \bar{u}_2&=K_{pq}(\tilde{u}_2-\hat{\phi}_{dr}i_{qs})+K_{iq}\int_0^t(\tilde{u}_2-\hat{\phi}_{dr}i_{qs})dt,\end{aligned} \tag{2.10}$$

where

$$\begin{aligned}\tilde{u}_1&=-K_{p\phi}\hat{\phi}_{dr}+K_{i\phi}\int_0^t(\phi_{dr}^*-\hat{\phi}_{dr})dt,\\ \tilde{u}_2&=-K_{p\omega}\omega_r+K_{i\omega}\int_0^t(\omega_r^*-\omega_r)dt.\end{aligned} \tag{2.11}$$

Here, ϕ_{dr}^*, ω_r^* represent the reference commands for ϕ_{dr}, ω_r, respectively. The constants $K_{i\phi}$, $K_{p\phi}$, K_{id}, K_{pd}, $K_{i\omega}$, $K_{p\omega}$, K_{iq}, and K_{pq} are controller gains. The roles of the PI controllers in (2.10) and IP controllers in (2.11) will soon be discussed.

In the following Theorem 2.1, we will show that under reasonable assumptions, the input-output dynamic responses of the induction motor with the controller consisting of (2.8)-(2.11) asymptotically follow those of the following decoupled linear system (2.6)' with some error bounds.

$$\begin{aligned}\dot{\bar{z}}_1&=A_1\bar{z}_1+b_1\phi_{dr}^*, & \bar{y}_1&=c_1\bar{z}_1,\\ \dot{\bar{z}}_2&=A_2\bar{z}_2+b_2\omega_r^*+ET_L, & \bar{y}_2&=c_2\bar{z}_2,\end{aligned} \tag{2.6'}$$

where the detailed structures of A_i, b_i, c_i, $i=1, 2$, and E are given in Appendix A. As can be seen from the block diagram representation of (2.6)' in Fig.2.1, the PI controllers in (2.10) are used to obtain fast speed and flux responses by controlling directly the torque and the d-axis stator current. Alternatively, high gain or hysteresis current controllers [6] may be used for the same purpose. On the other hand, the IP controllers in (2.11) are to assure the successful set-point tracking of commanded reference points ϕ_{dr}^*, ω_r^*. The IP controller provides better transient responses than the usual PI controller [24].

Before presenting Theorem 2.1, we need some preliminary developments. Let $x\triangleq[x_1\cdots x_{10}]^T$ where $x_1\triangleq i_{ds}$, $x_2\triangleq\phi_{dr}$, $x_3\triangleq\int(\phi_{dr}^*-\hat{\phi}_{dr})dt$, $x_4\triangleq\int(-K_{p\phi}\hat{\phi}_{dr}+K_{i\phi}x_3-i_{ds})dt$, $x_5\triangleq i_{qs}$, $x_6\triangleq\omega_r$, $x_7\triangleq\int(\omega_r^*-\omega_r)dt$, $x_8\triangleq\int(-K_{p\omega}\omega_r+K_{i\omega}x_7-\hat{\phi}_{dr}i_{qs})dt$, $x_9\triangleq\phi_{qr}$, and $x_{10}\triangleq\hat{\phi}_{dr}$. Let $u^*\triangleq[\phi_{dr}^*\ \omega_r^*]^T$ and $y\triangleq[\phi_{dr}\ \omega_r]^T$. Let $\Delta R_r=R_r-\hat{R}_r$, where $\hat{R}_r$ is the estimated value of R_r. Then, the closed-loop system consisting of (2.1), (2.2), and (2.8)-(2.11) can be written in the form:

$$\dot{x}=F(x)+G(x)\Delta R_r/R_r+Lu^*+\hat{E}T_L,\qquad y=Hx, \tag{2.12}$$

where the detailed structures of F, G, E, H, and L are given in Appendix A. Define the new state vector as $w\triangleq[z_1^T\ z_2^T\ e^T]^T=[z_{11}\cdots z_{14}\ z_{21}\cdots z_{24}\ e_1\ e_2]^T$. Through the state transformation:

$$w\triangleq T(x)=[x_1\ x_2\ x_3\ x_4\ (x_2x_5)\ x_6\ x_7\ x_8\ x_9\ (x_2-x_{10})]^T, \tag{2.13}$$

the system (2.12) is then transformed into

$$\dot{w}=\begin{bmatrix}\dot{z}_1\\ \dot{z}_2\\ \dot{e}\end{bmatrix}=\begin{bmatrix}A_1z_1+f_1(w)e+b_1\phi_{dr}^*+g_1(w)\Delta R_r/R_r\\ A_2z_2+f_2(w)e+b_2\omega_r^*+g_2(w)\Delta R_r/R_r+ET_L\\ f_3(w)e+g_3(w)\Delta R_r/R_r\end{bmatrix},$$

$$y_i=c_iz_i,\quad i=1,2, \tag{2.14}$$

where the detailed structures of A_i, b_i, c_i, $i=1, 2$, f_i, g_i, $i=1, 2, 3$, and E are given in Appendix A. The input-output dynamic characteristics of (2.14) are the same as those of (2.12) since only the state transformation (2.13) is involved between two systems (2.12) and (2.14). However, the system (2.14) has a simpler structure than the system (2.12). Therefore, the performance of our controller (2.8)-(2.11) can be studied more easily by using the system (2.14) instead of the original system (2.12). Note that, when $e=0$ (i.e. no estimation error of the rotor flux) and $\Delta R_r=0$ (i.e. no estimation error of the rotor resistance), the system (2.14) turns to the decoupled linear system (2.6)'.

For technical simplicity, we assume that

(A.1) For each $u_i^*:[0,\infty)\to\Omega_i$, $i=1, 2$, $T_L:[0,\infty)\to\Omega_T$ and $x(0)\in\Omega_x$, the system (2.12) has a unique solution $x:[0,\infty)\to\Omega_x$.

That is, we assume that the system (2.12) has a well-defined solution and is BIBS (Bounded Input - Bounded State) so that $x_2(=\phi_{dr})\neq0$ or $x_{10}(=\hat{\phi}_{dr})\neq0$. See Remark 2.1 for further comments on (A.1). Simple calculations show that all eigenvalues of A_1 and A_2 have negative real parts if the controller gains are chosen to satisfy the Routh-Hurwitz criterion:

$$n_{3i}(n_{1i}n_{2i}-n_{3i})-|n_{1i}|^2n_{4i}>0,\quad i=1,2, \tag{2.15}$$

where

$$
\begin{aligned}
&n_{11}=a_1+a_4+cK_{pq}+D/J,\\
&n_{21}=[(a_1+a_4)D+cK_{pq}(K_TK_{p\omega}+D)]/J+cK_{iq}\\
&n_{31}=[cK_TK_{i\omega}K_{pq}+cK_{iq}(K_TK_{p\omega}+D)]/J,\\
&n_{41}=cK_TK_{i\omega}K_{iq}/J, \qquad (2.16)\\
&n_{12}=a_1+a_5+cK_{pd},\\
&n_{22}=ca_4K_{pd}K_{p\phi}+ca_5K_{pd}+cK_{id}+a_1a_5-a_2a_4,\\
&n_{32}=ca_4K_{i\phi}K_{pd}+cK_{id}(a_4K_{p\phi}+a_5),\\
&n_{42}=ca_4K_{i\phi}K_{id},
\end{aligned}
$$

Therefore, we can assume that
(A.2) A_1 and A_2 are stable matrices.
Finally, we assume that
(A.3) There exists a constant $\alpha_r > 0$ such that

$$|\Delta R_r/R_r| \le \alpha_r. \qquad (2.17)$$

Let $\bar{e}=[\bar{e}_1^T \ \ \bar{e}_2^T]^T$ where $\bar{e}_i \triangleq z_i-\bar{z}_i$, $i = 1, 2$. From (2.6)' and (2.14),

$$
\begin{aligned}
&\dot{\bar{e}}_1=A_1\bar{e}_1+f_1(w)e+g_1(w)\Delta R_r/R_r, \quad y_1-\bar{y}_1=c_1\bar{e}_1,\\
&\dot{\bar{e}}_2=A_2\bar{e}_2+f_2(w)e+g_2(w)\Delta R_r/R_r, \quad y_2-\bar{y}_2=c_2\bar{e}_2, \qquad (2.18)\\
&\dot{e}=f_3(w)e+g_3(w)\Delta R_r/R_r.
\end{aligned}
$$

Since T, f_i, g_i, $i = 1, 2, 3$ are continuous and Ω_x is a compact subset of R^{10}, there exist positive constants α_i, and β_i such that

$$|f_i(w)| \le \alpha_i, \quad i=1,2 \quad \text{and} \quad |g_j(w)| \le \beta_j, \quad j=1,2,3. \qquad (2.19)$$

Let $Q_i \in R^{4\times4}$, $i = 1, 2$ be positive definite symmetric matrices. By (A.2), there exist positive definite matrices $P_i \in R^{4\times4}$, $i = 1, 2$ satisfying

$$A_i^TP_i+P_iA_i=-Q_i. \qquad (2.20)$$

Let

$$
\begin{aligned}
&\delta=\beta_3\alpha_r/a_4, \quad k_i=\lambda_m(Q_i)/(2\lambda_M(P_i)).\\
&d_{1i}=2\alpha_r\|P_i\|\lambda_M(P_i)(\beta_i+\alpha_i\beta_3/a_4)/\lambda_m(P_i)\lambda_m(Q_i),\\
&d_{2i}=\alpha_i(|e(0)|-\beta_3\alpha_r/a_4)\|P_i\|/\\
&\qquad \{\lambda_m(P_i)[\lambda_m(Q_i)/2\lambda_M(P_i)-a_4]\}, \qquad (2.21)\\
&d_{3i}=(\lambda_M(P_i)/\lambda_m(P_i))^{1/2}|\bar{z}_i(0)-z_i^s|, \quad i=1,2.
\end{aligned}
$$

Now, we are ready to state Theorem 2.1.

Theorem 2.1 Suppose that (A.1)-(A.3) are satisfied. Then, the controller (2.8)-(2.11) guarantees that, for all $t \ge 0$,

$$|e(t)| \le \delta+(|e(0)|-\delta)e^{-a_4t}, \qquad (2.22)$$

$$|y_i(t)-\bar{y}_i(t)| \le d_{1i}+d_{2i}e^{-a_4t}-(d_{1i}+d_{2i})e^{-k_it}, \quad i=1,2. \qquad (2.23)$$

In addition, if u^* and T_L are constant,

$$|y_i(t)-u_i^*| \le d_{1i}+d_{2i}e^{-a_4t}-(d_{1i}+d_{2i}-d_{3i})e^{-k_it}, \quad i=1,2. \qquad (2.24)$$

$$\omega_r^s=\omega_r^*, \quad \hat{\phi}_{dr}^s=\phi_{dr}^*. \qquad (2.25)$$

Theorem 2.1 states that the output responses of the induction motor with the controller (2.8)-(2.11) asymptotically follow those of the decoupled linear system (2.6)' with bounded errors. The estimation error of the rotor flux is also eventually confined to a certain bound. Since δ and d_{1i} are proportional to α_r, small estimation error of the rotor resistance is desirable for small "ultimate" bounds of $|e|$ and $|y - \bar{y}|$. An efficient identification algorithm for R_r will be presented in Section 3. The convergence rate of $|e|$ can be made faster by adopting the new flux observers [16,17] instead of the flux simulator (2.9). However, the convergence rate of the flux simulator (2.9) is fast enough for our purpose. The flux simulator and flux observers equally work well except for the first short period of system operation.

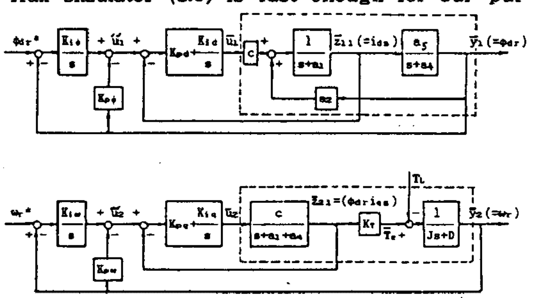

Fig.2.1. The block diagram representation of the decoupled linear system (2.6)'.

Remark 2.1 By (A.1), we priorly assumed that the closed-loop system (2.12) is BIBS. By (A.2), the decoupled linear system (2.6)' is also BIBS. Under these assumptions, Theorem 2.1 describes how the deviation of output responses of the closed-loop system (2.12) from the desired one (i.e. output responses of the decoupled linear system (2.6)') depends on the estimation error of the rotor resistance. The assumption (A.1) was made only for technical simplicity. It can be removed by imposing restrictions on the allowable sizes of Ω_1, Ω_2, Ω_T, and $|x(0)|$. However, the statement and proof of Theorem 2.1 get considerably complicated.

Next, we show how the controller (2.8)-(2.11) can be used to control induction motors with high power efficiency as well as high dynamic performance. Recently, Kusko and Galler [20], Park and Sul [21], and Murata et al. [22] found that, in the steady state, (i) there is an optimal slip angular speed ω_{sl}^* for maximal power efficiency and (ii) ω_{sl}^* is a function of ω_r (that is, $\omega_{sl}^*=f(\omega_r)$). The function $f(\omega_r)$ is usually obtained experimentally rather than analytically. The above results suggest that, to achieve maximal power efficiency in the steady state, the slip angular speed should be adjusted according to the relationship $\omega_{sl}^*=f(\omega_r)$. To do so, we generate the rotor flux command ϕ_{dr}^* in the following manner.

$$
\phi_{dr}^*=\begin{cases} |\hat{a}_5(K_{i\omega}x_7^s-K_{p\omega}\omega_r^*)/f(\omega_r^*)|^{1/2} & \text{if the system reaches the steady state,}\\ \text{the rated value of } \phi_{dr}, & \text{otherwise.}\end{cases} \qquad (2.26)
$$

Note that $x_7=z_{23}=\int(\omega_r^*-\omega_r)dt$ is accessible and recall that, if the system (2.12) reaches the steady state, $\omega_r^s=\omega_r^*$. We have chosen ϕ_{dr}^* as a piecewise constant function. However, such a step change in ϕ_{dr}^* will not significantly affect the rotor speed response since the dynamic characteristics of the induction motor with the controller (2.8)-(2.11) closely follow those of the decoupled linear system (2.6)', as is shown in Theorem 2.1.

If ϕ_{dr}^* is chosen as (2.26), the slip angular speed can be kept around the optimal slip angular speed in the steady state.

$$|1/\omega_{sl}^s-1/\omega_{sl}^*| \le [(1+K_{i\omega})d_{12}/\omega_{sl}^*+\delta\phi_{dr}^*/a_5]/|z_{21}^s| \qquad (2.27)$$

From (2.27), we can see that if there is no estimation error of the rotor resistance, d_{12} and δ are reduced to zero and hence $\omega_{sl}^s = \omega_{sl}^*$ is achieved.

3. Identification algorithm for the rotor resistance

In this section, we present an identification method for the rotor resistance. Other parameters of the induction motor are assumed to be insensitive to the machine temperature and to be priorly known. We also assume that the machine temperature varies slowly. All these assumptions are reasonable.

Suppose that the closed-loop system (2.12) is in the steady state. Then, the following relationships hold.

$$
\begin{aligned}
&\omega_{sl}^s=\hat{a}_5i_{qs}^s/\phi_{dr}^*, \quad \omega_s^s=p\omega_r^*+\omega_{sl}^s, \quad i_{ds}^s=\phi_{dr}^*/M,\\
&\phi_{dr}^s=\phi_{dr}^*+\phi_{qr}^s\omega_{sl}^s/a_4, \quad \phi_{qr}^s=\Delta R_ra_4\omega_{sl}^s\phi_{dr}^*/(|a_4|^2+|\omega_{sl}^s|^2)R_r, \qquad (3.1)
\end{aligned}
$$

and

$$
\begin{aligned}
&\bar{u}_1^s=R_si_{ds}^s-M\omega_s^s\phi_{qr}^s/L_r, \quad \bar{u}_2^s=\phi_{dr}^*[R_si_{qs}^s\\
&\qquad +L_s\omega_{sl}^si_{ds}^s+M\omega_s^s(\phi_{dr}^s-\phi_{dr}^*)/L_r]. \qquad (3.2)
\end{aligned}
$$

Now, define functions P and P^* by

$$
\begin{aligned}
&P=-a_5\omega_s^s(\phi_{dr}^si_{ds}^s+\phi_{qr}^si_{qs}^s)/R_r,\\
&P^*=-a_5\omega_s^s\phi_{dr}^*i_{ds}^s/R_r. \qquad (3.3)
\end{aligned}
$$

Then, using (3.1) and (3.3), we can express ZP as:

$$\Delta P=P-P^*=-\Delta R_r\omega_s^s|\omega_{sl}^s\phi_{dr}^*|^2(a_4+\hat{a}_4)/|R_r|^2(|a_4|^2+|\omega_{sl}^s|^2) \qquad (3.4)$$

This equation indicates that ΔP can be used as a correcting function for the adaptation of R_r [19]. In the case of no uncertainty in R_r, ΔP will be zero. Otherwise, ΔP will exist. However, (3.4) relates ΔP to ΔR_r implicitly. An explicit relationship between ΔR_r and ΔP can be obtained by refining the above result further. Insert the identity: $a_4 = \hat{a}_4 + (\hat{a}_4 \Delta R_r / R_r)$ into (3.4). Then, some manipulations of the resulting equation yield the following equation for ΔR_r.

$$(\Delta R_r / L_r)^2 + 2\hat{a}_4 (\Delta R_r / L_r) - K_0 = 0, \tag{3.5}$$

where

$$K_0 = -K_1 K_2 / (1+K_1), \quad K_1 = \Delta P |\hat{R}_r|^2 / L_r \omega_s^s |\omega_{s1}^s \phi_{dr}^*|^2, \quad K_2 = |\hat{a}_4|^2 + |\omega_{s1}^s|^2. \tag{3.6}$$

Solving (3.5), we finally get the explicit relationship between ΔR_r and ΔP:

$$\Delta R_r = -\hat{R}_r + \sqrt{|\hat{R}_r|^2 + |L_r|^2 K_0} \quad \text{or} \quad R_r = \sqrt{|\hat{R}_r|^2 + |L_r|^2 K_0}. \tag{3.7}$$

On the other hand, using (3.2) and (3.3), we obtain an alternative expression of ΔP:

$$\Delta P = \bar{u}_1^s i_{qs}^s - \bar{u}_2^s / M + L_s \omega_{s1}^s |i_{ds}^s|^2. \tag{3.8}$$

This equation can be used to compute ΔP since all variables that appear in (3.8) are accessible or known.

Using the above results, we can construct the identification algorithm for R_r. First, check if the closed-loop system (2.12) is in the steady state. If so, the steady-state values of $\bar{u}_1$, $\bar{u}_2$, ω_{s1}, and i_{ds} are all known. From these data and (3.8), K_0 in (3.6) can be calculated. In the presence of measurement noises, we would rather take the average value of K_0 over several sampling periods. Next, the new value of $\hat{R}_r$ is determined by (3.7), the calculated value of K_0, and the present value of $\hat{R}_r$. Finally, the constants $\hat{a}_1$, $\hat{a}_5$ that are needed for the execution of the controller (2.8)-(2.11) are updated by using this new value of $\hat{R}_r$.

4. Simulation and experimental results

Performances of the control scheme developed in the preceding sections were investigated by simulations and experiments. A 4 pole squirrel-cage induction motor was chosen for experimental work. The motor data are listed in Table 4.1. The controller gains used in the simulations and experiments are

$$K_{p\phi} = 81.8, \quad K_{i\phi} = 806.0, \quad K_{pd} = 5.0, \quad K_{id} = 5.0,$$
$$K_{p\omega} = 0.8, \quad K_{i\omega} = 6.3, \quad K_{pq} = 5.0, \quad K_{iq} = 5.0.$$

The block diagram of the speed drive system implemented for experimental work is shown in Fig.4.1. Our control scheme was implemented on the Motorola 68000 microprocessor and was executed every 0.5 ms. Signals between the microprocessor and the induction motor are processed through 12 bit A/D converters, 12 bit D/A converters, and 6821 peripheral interface adapters. The rotor speed and position are detected by 6840 counter/timers and an optical encoder whose resolution is 4000 pulses/rev. For load test, a DC generator was coupled with the induction motor. Its rated power and speed are 2.2 kW and 1750 rpm, respectively.

In practice, the optimal slip speed function $f(\omega_r^*)$ is obtained experimentally. Here, we attempt not to find $f(\omega_r^*)$ but to show the feasibility of our control scheme for high power efficiency. Accordingly, we assumed without loss of generality that $\omega_{sl}^* = 6.7, 34, 88$ rpm for $\omega_r^* = 100, 750, 1600$ rpm, respectively. In both simulations and experiments, $\hat{R}_r$ was initially assumed to be 0.42 Ω corresponding to a 50 % estimation error in R_r. At the initial time, the induction motor was being driven with no load at 100 rpm.

In this situation, ω_r^* was switched from 100 rpm to 750 rpm. To provide maximal power efficiency in the steady state, ϕ_{dr}^* was adjusted according to (2.35). The simulation and experimental results for this case are shown in Fig.4.2(a) and (b), respectively. The experimental results in Fig.4.2(b) are in good match with the simulation results in Fig.4.2(a). From Fig.4.2, we see that, in the presence of large estimation error in R_r, the actual responses of the rotor speed and rotor flux deviate much from the desired ones. Observe that the rotor speed response is affected by the change in ϕ_{dr} and that the slip speed in the steady state is different from the optimal slip speed. Thus, neither high dynamic performance nor maximal power efficiency can not be successfully achieved without good estimation of the rotor resistance.

After the system reached its steady state, the identification algorithm for R_r described in Section 3 was executed. Then, ω_r^* was switched from 750 rpm to 1600 rpm. The simulation results are shown in Fig.4.3(a). Since no measurement errors were assumed in the simulation, the identification algorithm produced the exact value of R_r. Accordingly, the simulation results in Fig.4.3(a) correspond to the case of no estimation error in R_r. Recall that, in the case of $\Delta R_r = 0$, the system eventually possesses the input-output dynamic characteristics of the decoupled linear system (2.6)'. We see that the step change in ϕ_{dr}^* made for power efficiency does not disturb the rotor speed response at all. In the experiment, the identification algorithm for R_r estimated the value of the rotor resistance as 0.89 Ω, which deviates 5.6 % from its nominal value given in Table 4.1. However, the experimental results shown in Fig.4.3(b) confirm that our control scheme is useful in controlling induction motors with maximal power efficiency as well as high dynamic performance.

Finally, we applied the rated load torque 12 Nm for 1 second at the rated rotor speed and flux. The simulation and experimental results in Fig.4.4 show that while the rotor speed response promptly recovers its commanded value, the rotor flux response is not affected by the load torque.

As can be seen from Fig.4.2-Fig.4.4, the experimental results agree well with the simulation results. However, there exist slight differences between the simulation and experimental results, which may result from two main reasons. First, the control algorithm was performed through 16 bit word operations in the microprocessor, so there exist quantization errors, roundoff errors, and truncation errors. Second, our identification algorithm for the rotor resistance depends on other parameters of the induction motor as well as measurement noises.

5. Conclusion

Through mathematical performance analyses, simulations, and experiments, we have shown that the recently developed nonlinear feedback control theories are practically useful in controlling the induction motor with high dynamic performance and maximal power efficiency. Most of the existing nonlinear feedback control theories in general require all state feedback variables to be accessible and all system parameters to be known with reasonable accuracy. In this paper, these limitations were overcome by using a rotor flux simulator and a parameter adaptation algorithm. Our control scheme can be easily modified for decoupling control of the motor torque and the rotor flux.

NOMENCLATURE

V_{ds} (V_{qs})	d-axis (q-axis) stator voltage
i_{ds} (i_{qs})	d-axis (q-axis) stator current
ϕ_{dr} (ϕ_{qr})	d-axis (q-axis) rotor flux
ω_r	rotor angular speed
ω_{s1}	slip angular speed
ω_{s1}^*	optimal slip angular speed for maximum power efficiency
R_s (R_r)	stator (rotor) resistance
L_s (L_r)	stator (rotor) self-inductance
M	stator/rotor mutual inductance
p	number of pole pairs
σ	$1 - M^2/L_s L_r$: leakage coefficient
c	$1/\sigma L_s$
a_1 ($\hat{a}_1$)	$c(R_s + M^2 R_r / L_r^2)$ ($c(R_s + M^2 \hat{R}_r / L_r^2)$)
a_2 ($\hat{a}_2$)	cMR_r / L_r^2 ($cM\hat{R}_r / L_r^2$)
$a_3 = \hat{a}_3$	cM/L_r
a_4 ($\hat{a}_4$)	R_r / L_r ($\hat{R}_r / L_r$)
a_5 ($\hat{a}_5$)	MR_r / L_r ($M\hat{R}_r / L_r$)
J	rotor inertia of the MG set
D	damping coefficient of the MG set
K_T	$3pM/2L_r$: torque constant
T_L	disturbance torque
$\|x\|$	Euclidean norm of $x \in R^n$
$\|A\|$	induced norm of a matrix A
x_i, u_i, y_i	i-th components of the vectors x,u,y
z_{ij}	j-th component of the vector z_i
z_i^s	steady state value of the vector z_i
Ω_1, Ω_2	compact subsets of R
Ω_x	compact subset of R^{10} such that $\Omega_x \cap \{x \in R^{10} : x_2 = 0 \text{ or } x_{10} = 0\} = \phi$
$\lambda_m(Q)$ ($\lambda_M(Q)$)	minimum(maximum) eigenvalue of a symmetric matrix Q

Table 4.1. Data of the induction motor used for experiment.

220V/380 V, 60 Hz, Delta-Connected Stator			
R_s	0.687 Ω	R_r	0.842 Ω
L_s	83.97 mH	L_r	85.28 mH
M	81.36 mH	J	0.03 Kgm^2
D	0.01 Kgm^2/s	ϕ_{dr}(rated)	0.48 Wb
i_{ds}(rated)	5.9 A	i_{qs}(rated)	11 A
rated power	2.2 kW	rated speed	1750 rpm

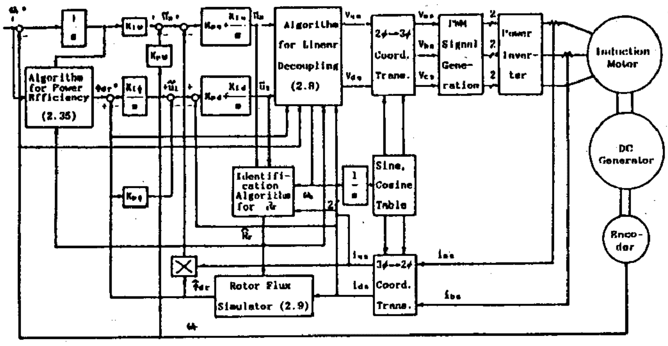

Fig.4.1. Block diagram of the implemented speed drive system.

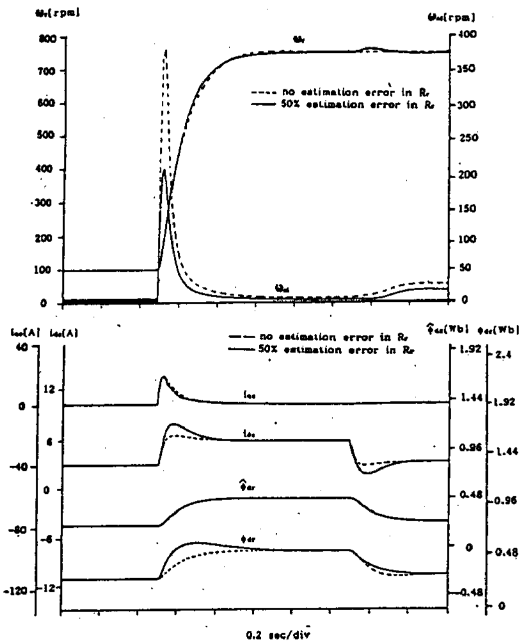

Fig.4.2.(a) Simulation results for the case of a 50 % estimation error in R_r.

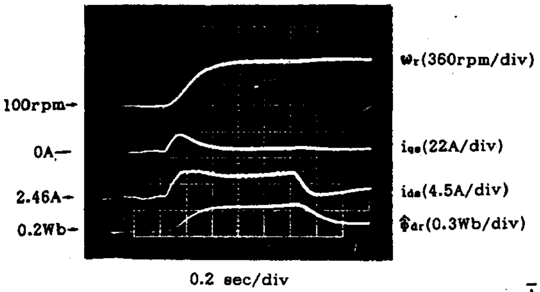

Fig.4.2.(b) Experimental results for the case of a 50 % estimation error in R_r.

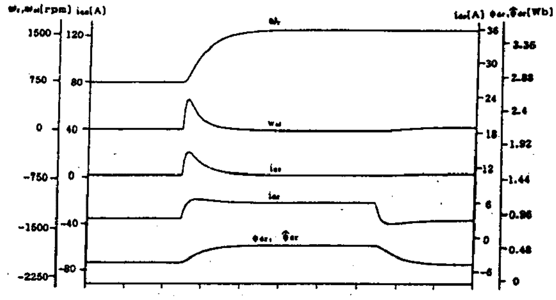

Fig.4.3.(a) Simulation results for the case of the parameter adaptation.

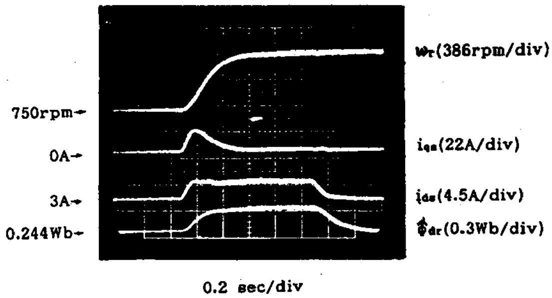

Fig.4.3.(b) Experimental results for the case of the parameter adaptation.

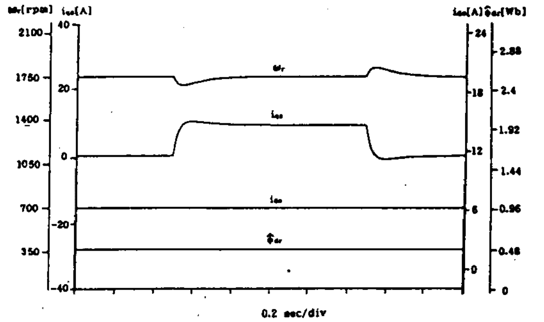

Fig.4.4.(a) Simulation results for a rectangular load torque.

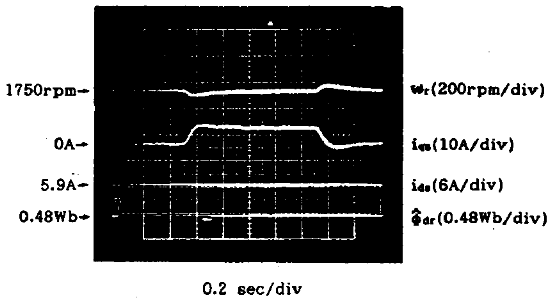

Fig.4.4.(b) Experimental results for a rectangular load torque.

APPENDIX A

(1) $\overline{A}_i$, $\overline{b}_i$, $\overline{c}_i$, i = 1, 2, and $\overline{E}$ in (2.6):

$$\overline{A}_1 = \begin{bmatrix} -a_1 & a_2 \\ a_5 & -a_4 \end{bmatrix},\ \overline{A}_2 = \begin{bmatrix} -(a_1+a_4) & 0 \\ K_T/J & -D/J \end{bmatrix},\ \overline{b}_1 = \begin{bmatrix} c \\ 0 \end{bmatrix},\ \overline{E} = \begin{bmatrix} 0 \\ -1/J \end{bmatrix},\ \overline{c}_1 = [0 \quad 1].$$

(2) F, G, $\hat{E}$, H, and L in (2.12):

$$F(x) = \begin{bmatrix} -(a_1+cK_{pd})x_1+a_2x_2+cK_{pd}K_{i\phi}x_3+cK_{id}x_4-cK_{pd}K_{p\phi}x_{10}+pa_3x_9x_6 \\ a_5x_1-a_4x_2+a_5x_3x_9/x_{10} \\ -x_{10} \\ -K_{p\phi}x_{10}+K_{i\phi}x_3-x_1 \\ -(a_1+cK_{pq})x_5+a_2x_9-pa_3x_6(x_2-x_{10})-\dfrac{a_5x_1x_5+cK_{pq}K_{p\omega}x_6-cK_{pq}K_{i\omega}x_7-cK_{iq}x_8}{x_{10}} \\ -Dx_6/J + K_T(x_2x_5-x_1x_9)/J \\ -x_6 \\ -K_{p\omega}x_6+K_{i\omega}x_7-x_{10}x_5 \\ a_5x_5-a_4x_9-a_5x_2x_5/x_{10} \\ a_5x_1-a_4x_{10} \end{bmatrix}$$

$$G(x) = \begin{bmatrix} 0 \\ -a_5x_5x_9/x_{10} \\ 0 \\ 0 \\ a_5x_1x_5/x_{10} \\ 0 \\ 0 \\ 0 \\ a_5x_2x_5/x_{10} \\ a_4x_{10}-a_5x_1 \end{bmatrix}, \quad L = \begin{bmatrix} 0 & 0 \\ 0 & 0 \\ 1 & 0 \\ 0 & 0 \\ 0 & 0 \\ 0 & 0 \\ 0 & 1 \\ 0 & 0 \\ 0 & 0 \\ 0 & 0 \end{bmatrix}, \quad \hat{E} = \begin{bmatrix} 0 \\ 0 \\ 0 \\ 0 \\ 0 \\ -1/J \\ 0 \\ 0 \\ 0 \\ 0 \end{bmatrix}, \quad H^T = \begin{bmatrix} 0 & 0 \\ 1 & 0 \\ 0 & 0 \\ 0 & 0 \\ 0 & 0 \\ 0 & 1 \\ 0 & 0 \\ 0 & 0 \\ 0 & 0 \\ 0 & 0 \end{bmatrix}.$$

(3) A_i, b_i, c_i, $i = 1, 2$, f_i, g_i, $i = 1, 2, 3$, and E in (2.6)' and (2.14)

$$A_1 = \begin{bmatrix} -(a_1+cK_{pd}) & a_2-cK_{pd}K_{p\phi} & cK_{pd}K_{i\phi} & cK_{id} \\ a_5 & -a_4 & 0 & 0 \\ 0 & -1 & 0 & 0 \\ -1 & -K_{p\phi} & K_{i\phi} & 0 \end{bmatrix}, \quad b_1 = \begin{bmatrix} 0 \\ 0 \\ 1 \\ 0 \end{bmatrix},$$

$$A_2 = \begin{bmatrix} -(a_1+a_4+cK_{pq}) & -cK_{pq}K_{p\omega} & cK_{pq}K_{i\omega} & cK_{iq} \\ K_T/J & -D/J & 0 & 0 \\ 0 & -1 & 0 & 0 \\ -1 & -K_{p\omega} & K_{i\omega} & C \end{bmatrix}, \quad E = \begin{bmatrix} 0 \\ -1/J \\ 0 \\ 0 \end{bmatrix}, \quad c_1^T = \begin{bmatrix} 0 \\ 1 \\ 0 \\ 0 \end{bmatrix},$$

$$f_1(w) = \left[\begin{array}{c:c} pa_3z_{22} & cK_{pd}K_{p\phi} \\ \dfrac{a_5z_{21}}{z_{12}(z_{12}-e_2)} & 0 \\ 0 & 1 \\ 0 & K_{p\phi} \end{array}\right], \quad f_3(w) = \left[\begin{array}{c:c} -a_4 & \dfrac{-a_5z_{21}}{z_{12}(z_{12}-e_2)} \\ \hdashline \dfrac{a_5z_{21}}{z_{12}(z_{12}-e_2)} & -a_4 \end{array}\right],$$

$$f_2(w) = \left[\begin{array}{c:c} \dfrac{a_5z_{21}^2}{z_{12}^2(z_{12}-e_2)} + a_2z_{12} & \begin{array}{c} c(K_{pq}K_{i\omega}z_{23}-K_{p\omega}K_{pq}z_{22}+K_{iq}z_{24})/(z_{12}-e_2) \\ - a_5z_{11}z_{21}/z_{12}(z_{12}-e_2) - pa_3z_{12}z_{22} \end{array} \\ -K_Tz_{11}/J & 0 \\ 0 & 0 \\ 0 & z_{21}/z_{12} \end{array}\right],$$

$$g_1(w) = \begin{bmatrix} 0 \\ \dfrac{-a_5z_{21}e_1}{z_{12}(z_{12}-e_2)} \\ 0 \\ 0 \end{bmatrix}, \quad g_2(w) = \begin{bmatrix} \dfrac{-a_5z_{21}^2e_1}{z_{12}^2(z_{12}-e_2)} + \dfrac{a_5z_{11}z_{21}}{z_{12}-e_2} \\ 0 \\ 0 \\ 0 \end{bmatrix},$$

$$g_3(w) = \begin{bmatrix} a_5z_{21}/(z_{12}-e_2) \\ -a_5z_{21}e_1/z_{12}(z_{12}-e_2) - a_4(z_{12}-e_2) + a_5z_{11} \end{bmatrix}.$$

References

[1] F. Blaschke, "The Principle of Field Orientation as Applied to the New TRANSVEKTOR Closed-Loop Control System for Rotating-Field Machines," Simens Review, Vol.34, pp.217-220 (1972).

[2] Y. Kuroe and H. Haneda, "Theory of Power-Electronic AC Motor Control for Modeling, Estimation, and Control and/or Analysis," Proc. of the 25th CDC, pp.54-61 (1986).

[3] M. Koyama et al., "Microprocessor-based Vector Control System for Induction Motor Drives with Rotor Time Constant Identification Function," IEEE Trans. Ind. Appl., Vol.21, No.3, pp.453-459 (1986).

[4] K. Ohnishi et al., "Decoupling Control of Secondary Flux and Secondary Current in Induction Motor Drive with Controlled Voltage Source and Its Comparison with Volts/Hertz Control," IEEE Trans. Ind. Appl., Vol.21, No.1, pp.241-246 (1985).

[5] R. D. Lorenz et al., "Performance of Feedforward Current Regulators for Field-Oriented Induction Machine Controllers," IEEE Trans. Ind. Appl., Vol.23, No.4, pp.597-602 (1987).

[6] E. Y. Y. Ho and P. C. Sen, "Decoupling Control of Induction Motor Drives," IEEE Trans. Ind. Elec., Vol.35, No.2, pp.253-262 (1988).

[7] A. D. Luca and G. Ulivi, "Full Linearization of Induction Motors via Nonlinear State-Feedback," Proc. of the 26th CDC, PP.1765-1770 (1987).

[8] Z. Krzeminski, "Nonlinear Control of Induction Motor," IFAC Conf. Rec., Vol.3, pp.349-354 (1987).

[9] D. I. Kim et al., "Asymptotic Decoupled Control of Rotor Speed and Rotor Flux in Induction Motors," SICE Conf. Rec., pp.847-851 (1988).

[10] A. Isidori et al., "Nonlinear Decoupling via Feedback: A Differential Geometric Approach," IEEE Trans. Automat. Contr., Vol.26, pp.331-345 (1980).

[11] B. Jakubczyk and W. Respondek, "On Linearization of Control Systems," Bull. Acad. Pol. Sci. Math., Vol.28, pp.517-520 (1980).

[12] L. R. Hunt et al., "Global Linearization of Nonlinear Systems," IEEE Trans. Automat. Contr., Vol.28, pp.24-31 (1983).

[13] H. Nijmeijer, "Feedback Decomposition of Nonlinear Control Systems," IEEE Trans. Automat. Contr., Vol.28, pp.861-862 (1983).

[14] I. J. Ha, "The Standard Decomposition and Noninteracing Feedback Control of Nonlinear Control Systems," SIAM J Contr., Vol.26, pp.1235-1249 (1988).

[15] A. B. Plunkett, "Direct Flux and Torque Regulation in PWM Inverter-Induction Motor Drive," IEEE Trans. Ind. Appl., Vol.13, pp.139-146 (1977).

[16] Y. Hori et al., "A Novel Induction Motor Flux Observer and Its Application to a High Performance AC Drive System," IFAC Conf. Rec., Vol.3, pp.355-360 (1987).

[17] G. C. Verghese and S. R. Sanders, "Observers for Flux Estimation in Induction Machines," IEEE Trans. Ind. Elec., Vol.35, No.1, pp.85-94 (1988).

[18] R. Krishnan and F. C. Doran, "Study of Parameter Sensitivity in High Performance Inverter-Fed Induction Motor Drive," IEEE Trans. Energy Conver., Vol.2, pp.70-75 (1987).

[19] L. J. Garces, "Parameter Adaptation for the Speed-Controlled Static AC Drive with a Squirrel-Cage Induction Motor," IEEE Trans. Ind. Appl., Vol.16, pp.173-178 (1980).

[20] A. Kusko and D. Galler, "Control Means for Minimization of Losses in AC and DC Motor Drives," IEEE Trans. on Ind. Appl., Vol.19, No.4, pp.561-570 (1983).

[21] M. H. Park and S. K. Sul, "Microprocessor-Based Optimal Efficiency Drive of an Induction Motor," IEEE Trans. Ind. Elec., Vol.20, No.6, pp.1453-1459 (1984).

[22] M. Murata et al., "A New Synthesis Met5hod for Efficiency Optimized Speed Control System Of Vector -Controlled Induction Machine," PESC'88, Vol.2, pp.862-869 (1988).

[23] T. J. Tarn et al., "Nonlinear Feedback in Robot Arm Control," Proc. of the 23th CDC, pp.736-751 (1984).

[24] P. K. Nandam and P. C. Sen, "A Comparative Study of Proportional-Integral(P-I) and Integral-Proportional(I-P) Controllers for DC Motor Drives," Int. J. Contr., Vol.44, No.1, pp.283-297 (1986).